HHS Public Access

Author manuscript

J Biomed Nanotechnol. Author manuscript; available in PMC 2017 December 01.

Published in final edited form as:

J Biomed Nanotechnol. 2016 December ; 12(12): 2172–2184. doi:10.1166/jbn.2016.2318.

Mucin-1-Antibody-Conjugated Mesoporous Silica Nanoparticles for Selective Breast Cancer Detection in a Mucin-1 Transgenic Murine Mouse Model

Didier Dréau[1,3,†], **Laura Jeffords Moore**[1,†], **Merlis P. Alvarez-Berrios**[2,‡], **Mubin Tarannum**[2,3], **Pinku Mukherjee**[1,3], and **Juan L. Vivero-Escoto**[2,3,*]

[1]Department of Biological Sciences, The University of North Carolina at Charlotte, 9201 University City Blvd, Charlotte NC 28223, USA

[2]Department of Chemistry, The University of North Carolina at Charlotte, Charlotte NC 28223, USA; 9201 University City Blvd, Charlotte NC 28223, USA

[3]The Center for Biomedical Engineering and Science, The University of North Carolina at Charlotte, Charlotte NC 28223, USA

Abstract

Mucin-1 (MUC1), a transmembrane glycoprotein is aberrantly expressed on ~90% of breast cancer and is an excellent target for nanoparticulate targeted imaging. In this study, the development of a dye-doped NIR emitting mesoporous silica nanoparticles platform conjugated to tumor-specific MUC1 antibody (ab-tMUC1-NIR-MSN) for *in vivo* optical detection of breast adenocarcinoma tissue is reported. The structural properties, the *in vitro* and *in vivo* performance of this nanoparticle-based probe were evaluated. *In vitro* studies showed that the MSN-based optical imaging nanoprobe is non-cytotoxic and targets efficiently mammary cancer cells overexpressing human tMUC1 protein. *In vivo* experiments with female C57BL/6 mice indicated that this platform accumulates mainly in the liver and did not induce short-term toxicity. In addition, we demonstrated that the ab-tMUC1-NIR-MSN nanoprobe specifically detects mammary gland tumors overexpressing human tMUC1 in a human MUC1 transgenic mouse model.

Keywords

Mucin-1; Mesoporous Silica Nanoparticles; Diagnosis; Breast Cancer; Transgenic Mouse Model

BACKGROUND

One of the most difficult challenges of oncology is to find effective target-specific methods for early tumor detection, which is critical for the success of cancer therapy. Tumor-associated mucin-1 protein (tMUC1) is an ideal candidate for a potential imaging target. Indeed, tMUC1 is a trans-membrane glycoprotein, which is overexpressed in almost all

*Author to whom correspondence should be addressed. jviveroe@uncc.edu.
†These two authors contributed equally to this publication.
‡Present address: Department of Science and Technology, Inter American University of Puerto Rico, Ponce, PR, USA.

human epithelial cell adenocarcinomas, including ~90% of human breast, ovarian, pancreatic, colorectal, lung, prostate, colon, and gastric carcinomas.[1–4] Other attractive features of tMUC1 include its ubiquitous distribution on the cell surface and its under-glycosylation in tumor cells. Aberrant glycosylation of MUC1 in breast carcinoma cells results in the availability and presentation of distinct epitopes not found in normal tissues.[1, 5, 6] Those epitopes allow the design of monoclonal antibodies that discriminate between normal and breast carcinoma cells. As tMUC1 is highly expressed (~90%) by cancer cells and observed early during in breast cancer progression, targeting MUC1 would allow for the development of both monitoring procedures and possible treatments for the vast majority of breast cancer patients.[4]

The present study utilizes the newly developed tMUC1 antibody (ab-tMUC1 named TAB-004™, Oncotab, Inc.) that recognizes and binds with a high binding affinity to a unique epitope within the tMUC1 tandem repeat sequence, along with the MUC1 transgenic murine model (MMT) system.[6–8] In this model, immunocompetent mice develop spontaneous mammary carcinomas, expressing the human tMUC1 tumor-associated antigen. This spontaneous model of breast cancer progression contrasts with models that are based on implantation of human tumor which are cell susceptible to genotype and phenotype drift following extended *in vitro* cell culture not to mention the absence of a fully functional immune system required when implanting human cells.[9] The limited predictive value of those immuno-compromised murine preclinical models in the development of nanoparticle-based platforms for diagnostic and therapy remains a major challenge. Although subcutaneously implanted tumor cells are useful for proof of principle studies, both their microenvironment and their progression toward metastasis are different.[9, 10] One remarkable advantage of the MMT model is that tumors develop spontaneously from normal cells in their natural tissue microenvironment in the presence of a viable immune system and further mimic the multiple stages observed in human cancer progression.[6, 8]

Nanotechnology has become one of the most active research fields in the last decades. Nanoparticles (NPs) have been extensively investigated for applications in both experimental and clinical settings to improve delivery efficiency of therapeutic and diagnostic agents.[11–15] Multifunctional nanocarriers have been applied to a wide variety of fields including, but not limited to, chemotherapy, gene delivery, immunotherapy, cardiovascular diseases, tissue engineering, theranostics and to circumvent the blood brain barrier.[11, 14, 16–22] In particular, nanoscale imaging contrast agents have attracted great attention because of their unique optical properties, high surface-to-volume ratio and tunable surface chemistry.[23–25] A diverse variety of nanoparticle-based MUC1-targeting platforms have been developed in the past years. Some of them use polymers, proteins, gold, iron oxide, and silica nanoparticles as the multifunctional imaging probes. These platforms have been functionalized with MUC1 antibodies and aptamers to target MUC1 antigen.[26–32] Nevertheless, very few reports have shown the *in vivo* application of tMUC1-targeted nanoparticles. Moore and co-workers developed a MUC1-target multimodal nanoprobe, which consisted of iron oxide nanoparticles and a NIR dye (Cy5.5) for magnetic resonance (MR) and NIR fluorescent imaging using small peptides as the targeting ligands. The *in vivo* MR and NIR imaging experiments on a xenograft model showed specific accumulation of the probe in tMUC1 positive tumors and virtually no signal in control tumors.[2] Shanehsazzadeh and co-workers

also reported on the development of dextran-coated iron oxide nanoparticles labeled with 99mTc and conjugated to the monoclonal antibody C595 for the specific detection of MUC1 positive cells *in vitro* and *in vivo*.[33] Despite the successful targeting of MUC1 positive cell lines (MDA-MB-231 and MCF-7) *in vitro*, the *in vivo* targeting results were disappointing. Dye-doped silica-based nanoparticles constitute very attractive platform to obtain efficient luminescent, stable, biocompatible and targeted nanoparticulate optical imaging agents for biomedical applications.[25, 34, 35] In particular, mesoporous silica nanoparticles (MSNs) have unique and favorable features such as large surface area and pore volume, low cytotoxicity, biocompatibility, chemical stability, ease of surface modification, and multi-functionality, make them suitable for a broad spectrum of biomedical applications.[36–38] Several MSN-based optical and multimodal probes have been developed in recent years.[34, 35, 39–44] Some of them have shown the successful incorporation of near-infrared (NIR) chromophores in MSN particles for *in vivo* optical imaging.[39, 45] Cai and co-workers have developed multimodal MSN-based nanoprobes for *in vivo* vasculature targeting. These MSN materials combined positron emission tomography (PET) and NIR fluorescent imaging.[46, 47] Wang, Zeng and co-workers also incorporated a NIR fluorophore (Cy754) into the framework of MSNs for mapping of sentinel lymph node by photo-acoustic and NIR fluorescent imaging.[48]

Here, we report the development of a tMUC1-specific dye-doped NIR fluorescent mesoporous silica nanoparticles (ab-tMUC1-NIR-MSN) platform for the optical detection *in vitro* and *in vivo* of breast carcinoma tissue overexpressing the human form of tMUC1. The MSN-based probe consists of a NIR cyanine dye (NIR-797) incorporated in the framework of the material and a tMUC-1 antibody (ab-tMUC1 named TAB-004™, Oncotab, Inc.) that is chemically attached to the surface of the particles through a poly (ethylene glycol) linker (Fig. 1). The experimental results from this study showed that ab-tMUC1-NIR-MSNs can efficiently target breast cancer overexpressing human tMUC-1 protein *in vitro* and *in vivo*.

METHODS

Chemicals

All reagents were purchased from Sigma-Aldrich (St. Louis, MO) and used without further purification; with the exception of polyethylene glycol 2,000 and NIR-797 isothiocyanate which were purchased from Alfa Aesar and Chemodex, respectively. The mouse monoclonal antibody recognizing the human tMUC1 antigen (TAB004™) was a generous gift of OncoTab Inc. Nano-W™ was purchased from Nanoprobes Inc.

Thermogravimetric Analysis (TGA)

TGA was carried out with a Mettler Toledo TGA/SDTA851 instrument equipped with a platinum pan and using a heating rate of 5 °C/min under nitrogen. The sample was heated up from 25 to 600 °C.

Scanning Electron Microscopy

A Raith 150 Field Emission Scanning Electron Microscope (SEM) was used to determine particle size and morphology. Each SEM sample was prepared by suspending the

nanoparticles in ethanol. A drop of the suspension was placed on a silicon wafer and the solvent was allowed to evaporate.

Transmission Electron Microscopy

A JEOL JEM 2100 LaB6 Transmission Electron Microscope (TEM) was used to corroborate particle size and morphology. Each TEM sample was prepared by suspending the nanoparticles in methanol. A drop of the suspension was placed on a TEM carbon grid 200 mesh and the solvent was allowed to evaporate overnight. For the negative-staining with Nano-W™ (Nanoprobes, Inc.), the dispersion of abMUC1-NIR-MSN material was dropped on the Lacey carbon grid and allowed to dry for few seconds, before the sample dried completely on the grid, one drop of the Nano-W™ was added. Another drop of Nano-W™ was added before the first drop dried. Finally, the grid was allowed to air dry for few hours before imaging with TEM.

Dynamic Light Scattering (DLS)

Dynamic DLS and zeta potential measurements were carried out using a Malvern Instrument Zetasizer Nano.

Surface Area and Pore Size

The N_2 sorption isotherms were determined in a NOVA 2200e Quantachrome surface area and pore size analyzer. The surface area was calculated using the BET method.

UV-Vis-NIR Absorption and Fluorescence Spectroscopy

The absorbance and fluorescence of the abMUC1-NIR-MSN material synthesized in this work were characterized by Cary 5000 UV-vis-NIR and Fluorolog spectrophotometers, respectively.

Flow Cytometry

A BD LSRFortessa™ cell analyzer was used for the fluorescence-activated cell sorting (FACS) experiments.

Confocal Microscopy

An Olympus Fluoview FV 1000 confocal fluorescence microscope system was used for the LCSM experiments.

In Vivo Imaging

The optical imaging was carried out by IVIS spectrum preclinical *in vivo* imaging system and the images were analyzed with Living Image® Software (PerkinElmer).

Synthesis of NIR797 Silane Derivative—The fluorochrome (NIR797 isothiocyanate; 5 mg; 5.7 μmol) was dissolved in 1.0 mL of dry dimethylformamide (DMF). Then 3-aminopropyl triethoxysilane (AP-TES) (5.2 μL; 28.4 μmol) was added and the solution was stirred for 3 h at room temperature under nitrogen atmosphere.

Synthesis of NIR-MSN Material—The as-synthesized solution of NIR-797 silane derivative was added to a dispersion of MSNs (100 mg in 20 mL of ethanol). The final mixture was stirred for 24 h at 90 °C in order to graft the NIR-797 silane compound onto the surface of MSNs. The NIR-MSN product was separated by centrifugation and re-dispersed in ethanol (15 mL). This procedure was repeated at least three times to remove any unbound NIR-797 silane chromophore. The total amount of unbound NIR-797 silane derivative was determined by UV-Visible-NIR spectrometry. The amounts of unreacted silane dye in the supernatant and washing solutions were collected and analyzed using UV-Visible-NIR spectrophotometry. The difference between the original and the unbound amount of NIR-797 silane compound accounts for the amount grafted to MSNs. Based on this procedure, the amount of NIR-797 grafted on the surface of MSNs was 30 nmol/mg.

Functionalization of NIR-MSN Material with Carboxy-PEG or Methoxy-PEG Silane Derivative—NIR-MSN particles (45 mg) were further modified by refluxing 50 mg of carboxy-PEG (CPEG) silane derivative in 20 mL of ethanol in the presence of 15 μL of NH_3 solution. The reaction flask was covered with aluminium foil and the dispersion was refluxed at 90 °C for 18 h. After that, the product was centrifuged and washed three times with ethanol. The final product (CPEG-NIR-MSNs) was stored in ethanol. As control sample, to evaluate the absence of MUC-1 antibody, NIR-MSNs were also functionalized with methoxy-PEG (MeOPEG) silane derivative following the protocol described above to produce MeOPEG-NIR-MSNs. The synthesis and characterization of both CPEG and MeOPEG silane heterobifunctional polymers has already been reported.[49]

Conjugation of the Anti-MUC1 Antibody (TAB-004™) with CPEG-NIR-MSN Material (ab-tMUC1-NIR-MSNs)—CPEG-NIR-MSN material was first washed with sterile water and 1 × phosphate buffer solution (PBS, GIBCO) to remove any ethanol solvent from the nanoparticles. The CPEG-NIR-MSNs (7.0 mg) were dispersed in 1 mL of PBS. The nanoparticle dispersion was mixed with the conjugation agent (1-ethyl-3-(3 dimethylaminopropyl) carbodiimide (EDC); 0.452 mg) and the anti-tMUC1 antibody TAB-004™ (1.0 mg).[7] The final mixture was stirred for 24 h at 2–8 °C. The suspension was then centrifuged and washed twice with PBS and stored in the same buffer solution at 4 °C in the dark until use. The supernatant and washing solutions were collected to assess the amount of tMUC1-antibody chemically attached to the MSN particles by using the BCA assay.

Synthesis of FITC-MSN Materials—To synthesize FITC-MSNs; firstly, the fluorophore (fluorescein isothiocyanate (FITC); 5 mg; 5.7 μmol) was dissolved in 1.0 mL of dry dimethylformamide (DMF). To this solution, 3-aminopropyl triethoxysilane (AP-TES) (5.2 μL; 28.4 μmol) was added and the solution was stirred for 3 hours at room temperature under nitrogen atmosphere. Following a similar procedure as the one described previously, the FITC dye was grafted to MSN material to afford FITC-MSN particles. This material was also functionalized with CPEG, MeOPEG and abMUC1 as described above.

Cells and Culture Conditions—Murine mammary epithelial cancer cells MMT and Mtag were derived from MMT and Mtag tumors, respectively. MMT tumors and cells

express the altered form of human tMUC1 antigen recognized by the MUC1 antibody. On the other hand, Mtag cells were derived from Mtag tumors that express the mouse form of MUC1, which is not recognized by MUC1 antibody.[4, 6, 8] Murine pancreatic ductal adenocarcinoma cells KCKO, which do not express tMUC1 antigen, are derived of PDA.MUC1KO mice.[50] MMT, Mtag and KCKO cells were cultured in Dulbecco's modified Eagle medium (DMEM) containing 10% fetal bovine serum, 1% non-essential amino acids, 1% of penicillin, 1% of streptomycin and supplemented with 1% of glutamine (all reagents obtained from Life Technologies). Cells were cultured in sterile conditions under high hygrometry (>85%), 5% CO_2 and at 37 °C. Cells were passaged when they reached 75 % of confluence.

Cell Cytotoxicity Assays—For cytotoxicity and internalization studies MSNs were labeled with fluorescein isothiocyanate molecule (ab-tMUC1-FITC-MSNs) following the same protocol as ab-tMUC1-NIR-MSNs. MMT and Mtag cells were seeded in a 96-well plate (5×10^3 cells/well) and incubated for 24 h in complete growth medium. Next, the growth medium was removed and cells were exposed to varying concentrations of ab-tMUC1-FITC-MSNs (6.25–500 μg/mL) diluted in growth medium. Following 48 h of incubation with nanoparticles, the supernatant including the nanoparticle solution was discarded and cells were washed twice with PBS buffer and allowed to recover in cell culture medium for 24 h at 37 °C under CO_2. After the recovery period, cytotoxicity measurements were performed using the CellTiter 96® AQueous Assay (Promega) in a spectrophotometer at 450 nm.

Internalization and Localization of ab-tMUC1-FITC-MSNs—For internalization studies, 2×10^5 cells were seeded in 6-well cell culture plates with glass slides and allowed to adhere for 24 h. After exposure to 100 μg/mL of abtMUC1-FITC-MSNs for 4 h, cells were washed twice with warm DMEM and stained with NucBlue® Live cell staining solution for 20 min at room temperature. Samples were washed twice with DMEM and microphotographs were taken using an Olympus Fluoview FV 1000 confocal fluorescence microscope. To determine the amount of nanoparticles internalized by cells, MMT, Mtag or KCKO cells were seeded at a density of 3×10^5 for 24 h incubation period and treated with 25 μg/mL of ab-tMUC1-FITC-MSNs for 2 h. After treatments, cells were washed twice with DMEM, detached (trypsin 0.2%) and resuspended in 1 × PBS buffer + 0.11% Trypan blue to quench the cell membrane adsorbed nanoparticles. Results are represented as FITC + cells (percentage of FITC + cells in the gated cell population) from 10,000 events of the cell samples exposed to 25 μg/mL of nanoparticles.

In Vivo Experiments—All animal experiments were performed in compliance with the policies and procedures of the Institutional Animal Care and Use Committee for animal treatment at UNC Charlotte. Adult (11 to 20 weeks old) female C57BL/6, Mtag and MMT mice with similar genetic background were used. The generation and maintenance of the mouse strains used in this study has been described earlier.[6, 8] Briefly, Mtag mice (C57BL/6 × MMTV-PyMT) express PyMT oncogene and develop spontaneous mammary tumors as early at 8–10 weeks of age. MMT mice (MUC1.Tg × MTag) express both the PyMT oncogene and human altered MUC1 (tMUC1). MMT mice developed spontaneous MUC1-

expressing mammary carcinomas with 100% penetrance at 8–15 weeks of age.[8] Critically, the tMUC1 (TAB-004™) antibody only recognizes the human form of tMUC1 but not the mouse form.[4]

The intravenous administration of the materials designed in this work was carried out by retro-orbital injections. This approach is less challenging than tail vein injections and reduces the distress in the animals.[51, 52] Moreover, it has been shown that the two routes of administration can be used interchangeably and are equally effective.[53, 54]

Biodistribution and Toxicity—The abdominal and thoracic regions of the female C57BL/6 mice were shaved to improve imaging resolution. Following retro-orbital injection of ab-tMUC1-NIR-MSNs at 16 mg/kg under anesthesia, the fluorescence distribution was monitored at days 1, 3, 4, 7 and 8 post-injection using the IVIS *in vivo* imaging system and the life science software (Perkins Elmer). After euthanasia, blood and organs such as liver, spleen, brain, lungs, kidneys and heart were collected and assessed for the presence of ab-tMUC1-NIR-MSN material's related fluorescence using the IVIS system. The biodistribution of ab-tMUC1-NIR-MSN was determined by fluorescence on organ lysates and is reported as fluorescence per gram of organ. Briefly, organs were collected and placed in lysis buffer supplemented with phosphatase inhibitor, and C-inhibitor, then homogenized using the IKA® T-25 high speed digital homogenizer. The fluorescence of each lysate was measured using a Bio-Tek Synergy HT microplate reader capable of reading in the near infrared range (700–800 nm). In addition, the potential for toxicity of the ab-tMUC1-NIR-MSNs was assessed in the plasma of mice through a panel of liver functions (i.e., total protein (g/dL), albumin (g/dL), total bilirubin (mg/dL), direct bilirubin (mg/dL), alkaline phosphatase (U/L), aspartate aminotransferase (AST; U/L) and alanine aminotransferase (ALT; U/L)) measured using a UniCel DxC 600/800 Synchron Clinical System (Beckman Coulter, Brea, CA).

Target Ability of ab-tMUC1-NIR-MSN Material In Vivo—For these experiments the mice were treated as mentioned in the section of biodistribution and toxicity. Following retro-orbital injection of ab-tMUC1-NIR-MSNs at 16 mg/kg under anesthesia, the fluorescence distribution and localization within tumor masses was monitored at 5 min, 4 h, 24 h and 48 h post-injection using the IVIS *in vivo* imaging system and the life science software (Perkins Elmer). After euthanasia, tumors and organs including liver, spleen, lungs, brain and kidney were collected and assessed for the presence of ab-tMUC1-NIR-MSN material's related fluorescence using the IVIS system.

Statistical Analysis—Data are presented as mean ± SEM unless noted. Differences between groups and treatments were assessed using one-way ANOVA and post-hoc test for comparison of 3 or more groups. Monitoring overtime was assessed by repeated measure ANOVA. Comparison between two groups were done using Student's test (two-tailed distribution). A priori, differences were considered significant at $P < 0.05$.

RESULTS

Synthesis and Characterization of ab-tMUC1-NIR-MSNs

The synthesis of ab-tMUC1-NIR-MSNs was carried out through a multi-step approach. MSNs were fabricated by using a modified surfactant-templated approach.[55] The surfactant was removed by calcination at 600 °C for 1 h. Structural properties of the MSN material were analyzed by N_2 sorption isotherms (BET method), dynamic light scattering (DLS), ζ-potential, scanning and transmission electron microscopy (SEM and TEM), and thermogravimetric analysis (TGA). The BET analysis showed that the MSN material had a surface area of 357.6 m^2/g (Table I). The hydrodynamic diameter of this material was 48.7 nm in phosphate buffer solution (PBS, pH 7.4, 1.0 mM). The surface of the MSNs was negatively charged due to the presence of deprotonated silanols on the surface of the nanoparticles as it is corroborated by the ζ-potential (−20.7 ± 1.3 mV) (Table I). SEM and TEM micrographs showed that the MSNs had sizes of 35.8 ± 5.8 nm in diameter (Figs. 2(A and B)). NIR-797 isothiocyanate chromophore was chemically modified to afford a NIR a silane derivative. This NIR silane compound was grafted onto MSN material under refluxing conditions in ethanol. NIR-797 dye was selected because it allows maximum skin penetration for *in vivo* optical experiments (λ_{ex} = 795 nm; λ_{em} = 817 nm). The amount of NIR-797 dye chemically attached to the MSNs was approximately 30.0 nmol/mg (2.8 wt.%) according to the UV-vis-NIR calculations. The amount of organic content was 8.7 wt.%, based on TGA data. This difference in organic content is due to the excess of AP-TES added together with the NIR silane derivative during the grafting reaction. The photophysical properties of NIR-MSN material were investigated by UV-Visible-NIR absorption and fluorescence spectroscopy. The results were compared with blank MSNs and the parent NIR-797 dye. As shown in Figure 2(C), the absorption of NIR-MSNs was similar to that of NIR-797. This is an indication that there was no major changes in the NIR chromophore upon incorporation in the framework of MSNs. Fluorescence spectroscopy measurements showed that the emission spectra of the NIR-MSN material is also similar to the NIR-797 chromophore without any significant spectral shifts (Fig. 2(D)). These results suggest that NIR-797 dye was successfully incorporated in MSNs without major influence in the photophysical properties of the parent chromophore. Moreover, strong fluorescence signal from NIR-MSN material was also identified with IVIS imaging system (Fig. 2(D) inset), which validates the potential ability of this MSN-based probe for *in vivo* optical imaging.

Carboxylic acid-PEG(CPEG)-silane polymer was grafted to the NIR-MSNs to generate the corresponding CPEG-NIR-MSN material. The BET analyses of PEGylated NIR-MSNs showed a reduction in the surface area which indicates the presence of the PEG molecules blocking the pores of MSN particles (Table I). The CPEG-NIR-MSN material showed a slight aggregation in PBS with hydrodynamic diameters of 95.2 nm. The slight decrease in the ζ-potential (−12.5 ± 0.3 mV) for the CPEG-NIR-MSN verifies the presence of the CPEG polymer molecules on the surface of MSN material. The CPEG polymer contains carboxylic acid groups which in PBS (1.0 mM, pH = 7.4) is deprotonated to form negatively charged carboxylate groups. TGA data was further confirmed the presence of PEG moieties on the surface of NIR-MSNs; as anticipated, the organic content of CPEG-NIR-MSNs increased 5.7%, in comparison with NIR-MSNs.

The structural properties of the MeOPEG-NIR-MSN control sample were also evaluated using the characterization techniques described above. The results, shown in Table I, indicate similar properties to those obtained for the CPEG-NIR-MSN nanoprobe.

CPEG-NIR-MSN particles were further functionalized with tMUC1 antibody (TAB004™) to generate ab-tMUC1-NIR-MSN material. MUC1-antibody was chemically attached to CPEG-NIR-MSNs by a coupling reaction mediated by EDC agent. The amount of tMUC1-antibody attached to the MSNs was quantified using BCA protein quantification assay. The quantity was determined by assessing the difference between the starting amounts of protein added to the conjugation reaction and the unreacted protein in the supernatant and washing solutions. Based on this method, the amount of tMUC1-antibody chemically attached to CPEG-NIR-MSNs was 30.9 ± 2.6 μg tMUC1-antibody per mg of MSN material. The presence of tMUC1 antibody on the surface of MSNs was also confirmed directly by negative-staining TEM. TEM grids containing ab-tMUC1-NIR-MSN material were prepared and stained with Nano-W™.[56] Figure 2(E) shows the TEM image of ab-tMUC1-NIR-MSNs negatively-stained with Nano-W. The dark spots (black arrows) depict the presence of ab-tMUC1 antibody, which are fairly homogeneously distributed throughout the nanoparticles.

Cytotoxicity and Internalization of ab-tMUC1-MSNs in Murine Mammary Epithelial MMT and Mtag Cancer Cells

The *in vitro* performance of the tMUC1-antibody conjugated MSN material were tested using nanoparticles labeled with fluorescein fluorophore (FITC). The structural properties of the FITC-labeled MSN materials are shown in Table I, the values obtained for these properties are similar to the NIR-labeled MSNs version. Nanoparticles-based contrast optical imaging agents should be biocompatible in a wide range of concentrations, the cytotoxicity of abtMUC1-FITC-MSNs was evaluated by exposing Mtag and MMT cells to increasing concentrations of ab-tMUC1-FITC-MSNs (0–500 μg/mL). Based on MTS assays, increasing ab-tMUC1-FITC-MSNs concentrations up to 500 μg/mL led to similar cell viability to those of cells incubated in absence of MSN material (Fig. 3). These data showed that the ab-tMUC1-FITC-MSN material may be safely used as contrast optical imaging agent *in vivo*. tMUC-1 is a cell-surface associated glycoprotein with high expression in the majority of the adenocarcinomas and, in particular, in primary and metastatic breast cancers.[1] In this work, we functionalized CPEG-FITC-MSNs with a novel monoclonal antibody that binds with high affinity to human tMUC-1 antigen. To confirm the specificity of ab-tMUC1-FITC-MSNs provided by the ab-tMUC1, internalization studies in Mtag, MMT and KCKO cells were carried out by flow cytometry. Mtag and MMT cells express the mouse and human homolog of MUC1 separately, and KCKO cells do not express MUC1 antigen at all.[50] The results showed that MMT cells engulfed more ab-tMUC1-FITC-MSNs compared to Mtag cells ($p < 0.0003$) and KCKO cells ($p < 0.0004$) (Fig. 4). These data support the ability of ab-tMUC1-FITC-MSNs to efficiently target the human tMUC1 in MMT cells. This observation was further confirmed by confocal microscopy. As shown in Figures 5(A–D), MMT cells readily internalized ab-tMUC1-FITC-MSN nanoprobe. Presumably, the internalization follows a target-specific endocytosis pathway as shown previously.[38] In contrast, with Mtag cells most of the material is not internalized and remains outside of the cell membrane (Figs. 5(E–H)). Furthermore; when the internalization

of control material MeOPEG-FITC-MSNs, which lacks the ab-tMUC1, was assessed by flow cytometry in MMT and Mtag cells, no statistically significant difference in internalization between both cell lines was observed (data not shown). This confirms that the presence of tMUC1 antibody enhances the internalization of ab-tMUC1-FITC-MSNs in MMT cells.

In Vivo Biodistribution and Toxicity of ab-tMUC1-NIR-MSN Material in Non-Tumor Bearing Mice

The first goal of the *in vivo* experiments was to determine the biodistribution and toxicity of ab-tMUC1-NIR-MSN nanoprobe. For this purpose, non-tumor bearing C57BL/6 mice were administered with 16 mg/kg of the MSN-based probe via retro-orbital injection and analyzed by optical imaging. Whole-body fluorescence analysis revealed a strong signal in the abdominal region 24 h after retro-orbital injection of ab-tMUC1-NIR-MSNs (image not shown); likely due to the accumulation of nanoparticles in the liver, as indicated by *ex vivo* imaging (Fig. 6). A similar biodistribution of the particles was detected after 72 h (Fig. 6(A)). To further investigate the extent of ab-tMUC1-NIR-MSN material accumulation in the abdominal region, we monitored the fluorescence distribution for up to 8 days *in vivo* (Fig. 6(B)). The kinetic of the fluorescent signal from ab-tMUC1-NIR-MSN particles in this region reaches the maximum intensity after day 4 post-injection. In the following days, the abdominal region showed an overall decrease of the signal compared to the fluorescence measured on day 4. These data confirmed the preferential location of ab-tMUC1-NIR-MSNs in the abdominal region and excretion of the material; likely, by the hepatobiliary pathway as reported previously.[39, 45] For *ex vivo* optical imaging analysis, organs such as liver, kidneys, heart, brain, spleen and lungs, mice were obtained on day 3 post retro-orbital injection of the ab-tMUC1-NIR-MSNs. *Ex vivo* NIR fluorescent imaging confirmed the biodistribution of ab-tMUC1-NIR-MSN nanoprobe in non-tumor bearing C57BL/6 mice (Fig. 6(C)). The liver showed the highest accumulation of particles followed by the spleen and lungs. Organs from a control mouse that has not been injected with the ab-tMUC1-NIR-MSN probe did not show any significant fluorescence.

The short-term toxicity was also evaluated for the group of mice described above. No alteration in animal behavior or animal weight was noted regardless of the mice (data not shown). As mentioned above, the *ex vivo* imaging demonstrated that ab-tMUC1-NIR-MSN nanoprobe accumulates mainly in the liver, which is the organ that may suffer major damage in the presence of the MSN probe.

To evaluate the toxicity in this organ, liver panels were conducted on the animals (Table II). The data indicated that the retro-orbital administration of ab-tMUC1-NIR-MSNs and further accumulation in liver after 8 days did not affect any of the parameters indicative of liver functions with the exception of a decrease in alkaline phosphatase activity and ALT. More importantly, the key markers of liver dysfunction or damage,[57] which are increases in AST or ALT concentrations were not observed. The data from Table II, together with previous reports demonstrated that ab-tMUC1-NIR-MSN nanoprobe is safe during a short-term period and it can be a promising candidate as optical contrast imaging nanoprobe for *in vivo* applications.[35, 36, 41]

In Vivo ab-tMUC1-NIR-MSN Material Recognizes the Human tMUC-1 Antigen

Dr. Mukherjee and collaborators have developed transgenic murine systems that include two mouse models, Mtag and MMT.[6, 8] Both mice spontaneously develop multiple mammary tumors. However, tumors in MMT mice express the human form of MUC1 and as the normal mammary gland becomes malignant, normal MUC1 changes to tMUC1 (similar to what is observed in human disease). This makes the MMT mice appropriate models to test the ab-tMUC1-NIR-MSN nanoprobe for targeted localization. Mice develop spontaneous human tMUC1-expressing mammary carcinomas with 100% penetrance by 8–15 weeks of age. This system was used to test the target capability of the ab-tMUC1-NIR-MSN nanoprobe. The nanoprobe markedly accumulated in the tumor tissue of MMT mouse as early as 5 min post-injection (Figs. 7(A–D), (right mouse)). Although the ab-tMUC1-NIR-MSN probe fluorescence weakens overtime presumably because of degradation and excretion,[39, 45] a significant accumulation of the nanoprobe in MMT tumor tissue remains up to 48 h post-injection. In contrast, the Mtag tumor tissue (i.e., control not expressing tMUC1 antigen) showed limited to no accumulation in tumor tissue *in vivo* (Figs. 7(A–D), (left mouse)). Interestingly, retro-orbital administration of MeOPEG-NIR-MSN material in MMT and Mtag mice did not show significant accumulation of the nanoprobe in tumor tissue (Figs. 7(E–H)). Non-targeted nanoparticles, such as the MeOPEG-NIR-MSNs, have been shown to accumulate in tumors through a passive mechanism also known as enhanced permeability and retention (EPR) effect.[36, 41] However, the presence of a targeting agent, like ab-tMUC1, in the surface of the nanoparticles complements and enhances their accumulation in tumors through an active targeting mechanism.[58]

To further corroborate the target ability of the MUC1-targeted MSN probe, the *ex vivo* fluorescence associated with ab-tMUC1-NIR-MSN material in the tumor tissue of Mtag and MMT mice ($n = 3$) were measured by the IVIS (Fig. 8(A)). The accumulation of ab-tMUC1-NIR-MSN nanoprobe within the tumor tissue was significantly higher in MMT-derived tumor mass compared to those of Mtag animals ($p = 0.0558$, Figs. 8(A and B)). The small amount of ab-tMUC1-NIR-MSN nanoprobe observed in the Mtag mouse derived tumor tissue mice may be due to the passive targeting of nanoparticles toward tumor mass through EPR effect.[36, 41] As expected, ab-tMUC1-NIR-MSN material also accumulated in similar amounts in the liver, spleen and kidneys of Mtag and MMT mice based on quantitative analysis of the protein lysates extracted from each organ (Table III). Similar to the biodistribution in non-tumor bearing C57BL/6 mice, the nanoprobe accumulated mostly in the liver. These results confirm that ab-tMUC1-NIR-MSN nanoprobe efficiently target the human tMUC-1 antigen in MMT tumors.

DISCUSSION

The transmembrane glycoprotein MUC1 is aberrantly glycosylated and overexpressed in a variety of epithelial carcinomas such as breast cancer. tMUC1 differs from the MUC1 expressed in normal cells with regard to its biochemical features, cellular distribution and function.[1–3] Nanoparticle-based target-specific optical imaging probes are an attractive tool for the selective detection of tMUC1 in breast cancer.[26–31] In this study, we have synthesized and characterized a tMUC1-specific MSN-based NIR optical contrast imaging platform. The

cytotoxicity and target-ability of the MSN material *in vitro* was determined using murine mammary carcinoma cell lines that express mouse (Mtag) and human (MMT) altered MUC1 glycoprotein. KCKO cells, which do not express tMUC1 antigen at all, were used as negative control. The ab-tMUC1-NIR-MSN optical nanoprobe did not present major cytotoxicity in concentrations up to 500 μg/mL (Fig. 3). Moreover, the nanoprobe is internalized in higher amounts in MMT cells as an indication of the efficient target capability of the system toward the human tMUC1 antigen (Figs. 4 and 5).

To characterize the *in vivo* performance of ab-tMUC1-NIR-MSNs, we tested the biodistribution and toxicity of ab-tMUC1-NIR-MSN in non-tumor bearing female C57BL/6 mice post retro-orbital injection (Fig. 6). The MSN-based optical probe mainly accumulated in the abdominal region, reaching the maximum peak of fluorescence after four days and decreasing thereafter, an indication that the material is being excreted from the mice. *Ex vivo* analysis of different organs demonstrated that the ab-tMUC1-NIR-MSN nanoprobe is mainly localized in the liver. Interestingly, with comparable values to those observed in normal mice,[59, 60] liver panels conducted in the animals did not show major short-term toxicity due to the presence of the ab-tMUC1-NIR-MSN probe in this organ (Table II). However, additional studies need to be conducted to evaluate the long-term toxicity of the ab-tMUC1-NIR-MSN nanoprobe. The results depicted in Tables II and III support and complement previous studies in mice showing that MSN materials accumulate mainly in liver without major toxic effects.[36, 37, 39, 45]

Previous reports have shown the capability of MUC1-target multimodal nanoprobes to specifically accumulate in tMUC1 positive tumors using a xenograft model.[2] However, to our knowledge, no report has been published on the ability of MUC1-target nanoparticles to selectively accumulate on tumor tissue overexpressing tMUC1 in orthotopic or genetically engineered mice models. Herein, we investigated the ability of the ab-tMUC1-NIR-MSN optical nanoprobe to detect and target breast tumors that express the human form of tMUC1 protein in a MUC1 transgenic mouse model (MMT). The data depicted in Figures 7 and 8 demonstrate that the ab-tMUC1-NIR-MSN nanoprobe accumulates in higher amount in tumors that overexpress the human tMUC1 glycoprotein (MMT tumors) compared with those that overexpress the mouse homolog of tMUC1 antigen (Mtag tumors).

In conclusion, our *in vivo* results in the MMT mouse model demonstrated that ab-tMUC1-NIR-MSN nanoprobe can successfully detect breast tumors overexpressing human tMUC1 protein. We envision that this MSN-based nanoprobe cannot only detect primary breast cancer tumors, but it may also be used to track metastatic breast tumors. Thus, this MSN-based optical probe has the potential to greatly aid in screening prospective patients for early breast tumors detection and in possibly monitoring the efficacy of drug therapy.

Acknowledgments

We thank the following funding sources for their support: the North Carolina Biotechnology Center (NCBC Loan# 2014-SRL-2604); The Center for Biomedical and Engineering Sciences (CBES) for a seed grant. Juan L. Vivero-Escoto was supported by UNC Charlotte (start-up funding), the Nanoscale Science Program at UNC Charlotte and NIH AREA grant 1R15CA192160-01. OncoTab Inc. is also acknowledged for the kind gift of the antibody TAB-004™. We also acknowledge Ms. Priyanka Grover for help with Mtag cells. We thank Dr. Lopamudra Das Roy for helpful discussion regarding to the MMT and MTag cells. Finally, we are thankful to Dr. Williams

(University veterinarian and Director of Laboratory animal resources) for her support and technical expertise with animal experiments.

References

1. Nath S, Mukherjee P. MUC1: A multifaceted oncoprotein with a key role in cancer progression. Trends Mol Med. 2014; 20:332. [PubMed: 24667139]
2. Moore A, Medarova Z, Potthast A, Dai G. *In vivo* targeting of underglycosylated MUC-1 tumor antigen using a multimodal imaging probe. Cancer Res. 2004; 64:1821. [PubMed: 14996745]
3. Cai L, Chen ZZ, Chen MY, Tang HW, Pang DW. MUC-1 aptamer-conjugated dye-doped silica nanoparticles for MCF-7 cells detection. Biomaterials. 2013; 34:371. [PubMed: 23084552]
4. Moore LJ, Roy LD, Zhou R, Grover P, Wu ST, Curry JM, Dillon LM, Puri PM, Yazdanifar M, Puri R, Mukherjee P, Dreau D. Antibody-guided *in vivo* imaging for early detection of mammary gland tumors. Trans Oncol. 2016; 9:295.
5. Ho SB, Niehans GA, Lyftogt C, Yan PS, Charwitz DL, Gum ET, Dahiya R, Kim YS. Heterogeneity of mucin gene expression in normal and neoplastic tissues. Cancer Res. 1993; 53:641. [PubMed: 7678777]
6. Chen D, Xia J, Tanaka Y, Chen H, Koido S, Wernet O, Mukherjee P, Gendler SJ, Kufe D, Gong J. Immunotherapy of spontaneous mammary carcinoma with fusions of dendritic cells and mucin 1-positive carcinoma cells. Immunology. 2003; 109:300. [PubMed: 12757626]
7. Curry JM, Thompson KJ, Rao SG, Besmer DM, Murphy AM, Grdzelishvili VZ, Ahrens WA, McKillop IH, Sindram D, Iannitti DA, Martinie JB, Mukherjee P. The use of a novel MUC1 antibody to identify cancer stem cells and circulating MUC1 in mice and patients with pancreatic cancer. J Surg Oncol. 2013; 107:713. [PubMed: 23335066]
8. Mukherjee P, Madsen CS, Ginardi AR, Tinder TL, Jacobs F, Parker J, Agrawal B, Longenecker BM, Gendler SJ. Mucin 1-specific immunotherapy in a mouse model of spontaneous breast cancer. J Immunother. 2003; 26:47. [PubMed: 12514429]
9. Green JE, Hudson T. The promise of genetically engineered mice for cancer prevention studies. Nat Rev Cancer. 2005; 5:184. [PubMed: 15738982]
10. HogenEsch H, Nikitin AY. Challenges in pre-clinical testing of anti-cancer drugs in cell culture and in animal models. J Controlled Release. 2012; 164:183.
11. Jia F, Liu X, Li L, Mallapragada S, Narasimhan B, Wang Q. Multifunctional nanoparticles for targeted delivery of immune activating and cancer therapeutic agents. J Controlled Release. 2013; 172:1020.
12. Yang Y, Wang S, Wang Y, Wang X, Wang Q, Chen M. Advances in self-assembled chitosan nanomaterials for drug delivery. Biotechnol Adv. 2014; 32:1301. [PubMed: 25109677]
13. Peng H, Liu X, Wang G, Li M, Bratlie KM, Cochran E, Wang Q. Polymeric multifunctional nanomaterials for theranostics. J Mater Chem B. 2015; 3:6856.
14. Song F, Li X, Wang Q, Liao L, Zhang C. Nanocomposite hydrogels and their applications in drug delivery and tissue engineering. J Biomed Nanotechnol. 2015; 11:40. [PubMed: 26301299]
15. Thambi T, Park JH. Recent advances in shell-sheddable nanoparticles for cancer therapy. J Biomed Nanotechnol. 2014; 10:1841. [PubMed: 25992443]
16. Li MH, Yu H, Wang TF, Chang ND, Zhang JQ, Du D, Liu MF, Sun SL, Wang R, Tao HQ, Geng SL, Shen ZY, Wang Q, Peng HS. Tamoxifen embedded in lipid bilayer improves the oncotarget of liposomal daunorubicin *in vivo*. J Mater Chem B. 2014; 2:1619.
17. Peng H, Wang C, Xu X, Yu C, Wang Q. An intestinal Trojan horse for gene delivery. Nanoscale. 2015; 7:4354. [PubMed: 25619169]
18. Cao J, Wang R, Gao N, Li M, Tian X, Yang W, Ruan Y, Zhou C, Wang G, Liu X, Tang S, Yu Y, Liu Y, Sun G, Peng H, Wang Q. A7RC peptide modified paclitaxel liposomes dually target breast cancer. Biomater Sci. 2015; 3:1545. [PubMed: 26291480]
19. Gozuacik D, Yagci-Acar HF, Akkoc Y, Kosar A, Dogan-Ekici AI, Ekici S. Anticancer use of nanoparticles as nucleic acid carriers. J Biomed Nanotechnol. 2014; 10:1751. [PubMed: 25992440]

20. Liu M, Li M, Sun S, Li B, Du D, Sun J, Cao F, Li H, Jia F, Wang T, Chang N, Yu H, Wang Q, Peng H. The use of antibody modified liposomes loaded with AMO-1 to deliver oligonucleotides to ischemic myocardium for arrhythmia therapy. Biomaterials. 2014; 35:3697. [PubMed: 24468403]
21. Du D, Chang N, Sun S, Li M, Yu H, Liu M, Liu X, Wang G, Li H, Liu X, Geng S, Wang Q, Peng H. The role of glucose transporters in the distribution of *p*-aminophenyl-α-D-mannopyranoside modified liposomes within mice brain. J Controlled Release. 2014; 182:99.
22. Li M, Deng H, Peng H, Wang Q. Functional nanoparticles in targeting glioma diagnosis and therapies. J Nanosci Nanotechnol. 2014; 14:415. [PubMed: 24730272]
23. Hahn MA, Singh AK, Sharma P, Brown SC, Moudgil BM. Nanoparticles as contrast agents for *in-vivo* bioimaging: Current status and future perspectives. Anal Bioanal Chem. 2011; 399:3. [PubMed: 20924568]
24. Choi HS, Frangioni JV. Nanoparticles for biomedical imaging: Fundamentals of clinical translation. Mol Imaging. 2010; 9:2910.
25. Montalti M, Prodi L, Rampazzo E, Zaccheroni N. Dyedoped silica nanoparticles as luminescent organized systems for nanomedicine. Chem Soc Rev. 2014; 43:4243. [PubMed: 24643354]
26. Danysh BP, Constantinou PE, Lukianova-Hleb EY, Lapotko DO, Carson DD. The MUC1 ectodomain: A novel and efficient target for gold nanoparticle clustering and vapor nanobubble generation. Theranostics. 2012; 2:777. [PubMed: 22916077]
27. Ghasemi Z, Dinarvand R, Mottaghitalab F, Esfandyari-Manesh M, Sayari E, Atyabi F. Aptamer decorated hyaluronan/chitosan nanoparticles for targeted delivery of 5-fluorouracil to MUC1 over-expressing adenocarcinomas. Carbohydr Polym. 2015; 121:190. [PubMed: 25659689]
28. Hasegawa M, Sinha RK, Kumar M, Alam M, Yin L, Raina D, Kharbanda A, Panchamoorthy G, Gupta D, Singh H, Kharbanda S, Kufe D. Intracellular targeting of the oncogenic MUC1-C protein with a novel GO-203 nanoparticle formulation. Clin Cancer Res. 2015; 21:2338. [PubMed: 25712682]
29. Jo H, Her J, Ban C. Dual aptamer-functionalized silica nanoparticles for the highly sensitive detection of breast cancer. Biosens Bioelectron. 2015; 71:129. [PubMed: 25897882]
30. Kouchakzadeh H, Shojaosadati SA, Mohammadnejad J, Paknejad M, Rasaee MJ. Attachment of an anti-MUC1 monoclonal antibody to 5-FU loaded BSA nanoparticles for active targeting of breast cancer cells. Hum Antibodies. 2012; 21:49. [PubMed: 23549021]
31. Sayari E, Dinarvand M, Amini M, Azhdarzadeh M, Mollarazi E, Ghasemi Z, Atyabi F. MUC1 aptamer conjugated to chitosan nanoparticles, an efficient targeted carrier designed for anticancer SN38 delivery. Int J Pharm. 2014; 473:304. [PubMed: 24905777]
32. Yu C, Hu Y, Duan J, Yuan W, Wang C, Xu H, Yang XD. Novel aptamer-nanoparticle bioconjugates enhances delivery of anticancer drug to MUC1-positive cancer cells *in vitro*. PLoS One. 2011; 6:e24077. [PubMed: 21912664]
33. Shanehsazzadeh S, Gruettner C, Lahooti A, Mahmoudi M, Allen BJ, Ghavami M, Daha FJ, Oghabian MA. Monoclonal antibody conjugated magnetic nanoparticles could target MUC-1-positive cells *in vitro* but not *in vivo*. Contrast Media Mol Imaging. 2015; 10:225. [PubMed: 25327822]
34. Vivero-Escoto JL, Huxford-Phillips RC, Lin W. Silica-based nanoprobes for biomedical imaging and theranostic applications. Chem Soc Rev. 2012; 41:2673. [PubMed: 22234515]
35. Caltagirone C, Bettoschi A, Garau A, Montis R. Silica-based nanoparticles: A versatile tool for the development of efficient imaging agents. Chem Soc Rev. 2015; 44:4645. [PubMed: 25406516]
36. He Q, Shi J. Mesoporous silica nanoparticle based nano drug delivery systems: Synthesis, controlled drug release and delivery, pharmacokinetics and biocompatibility. J Mater Chem. 2011; 21:5845.
37. He Q, Shi J. MSN anti-cancer nanomedicines: Chemotherapy enhancement, overcoming of drug resistance, and metastasis inhibition. Adv Mater. 2014; 26:391. [PubMed: 24142549]
38. Vivero-Escoto JL, Slowing II, Trewyn BG, Lin VSY. Mesoporous Silica Nanoparticles for Intracellular Controlled Drug Delivery. Small. 2010; 6:1952. [PubMed: 20690133]
39. Lee CH, Cheng SH, Wang YJ, Chen YC, Chen NT, Souris J, Chen CT, Mou CY, Yang CS, Lo LW. Near-infrared mesoporous silica nanoparticles for optical imaging: Characterization and *in vivo* biodistribution. Adv Funct Mater. 2009; 19:215.

40. Hu X, Wang M, Miao F, Ma J, Shen H, Jia N. Regulation of multifunctional mesoporous core–shell nanoparticles with luminescence and magnetic properties for biomedical applications. J Mater Chem B. 2014; 2:2265.
41. Gandhi S, Thandavan K, Kwon BJ, Woo HJ, Yi SS, Lee HS, Jeong JH, Jang K, Shin DS. Mesoporous silica. A highly promising and compatible candidate for optical and biomedical applications. RSC Adv. 2014; 4:5953.
42. Palantavida S, Tang R, Sudlow GP, Akers WJ, Achilefu S, Sokolov I. Ultrabright NIR fluorescent mesoporous silica nanoparticles. J Mater Chem B. 2014; 2:3107.
43. Tao L, Song C, Sun Y, Li X, Li Y, Jin B, Zhang Z, Yang K. A fluorescent and chemiluminescent difunctional mesoporous silica nanoparticle as a label for the ultrasensitive detection of cancer cells. Anal Chim Acta. 2013; 761:194. [PubMed: 23312331]
44. Ma K, Sai H, Wiesner U. Ultrasmall sub-10 nm near-infrared fluorescent mesoporous silica nanoparticles. J Am Chem Soc. 2012; 134:13180. [PubMed: 22830608]
45. Souris JS, Lee CH, Cheng SH, Chen CT, Yang CS, Ho JAA, Mou CY, Lo LW. Surface charge-mediated rapid hepatobiliary excretion of mesoporous silica nanoparticles. Biomaterials. 2010; 31:5564. [PubMed: 20417962]
46. Chen F, Nayak TR, Goel S, Valdovinos HF, Hong H, Theuer CP, Barnhart TE, Cai W. *In Vivo* tumor vasculature targeted PET/NIRF imaging with TRC105(Fab)-conjugated, dual-labeled mesoporous silica nanoparticles. Mol Pharmaceutics. 2014; 11:4007.
47. Chen F, Hong H, Goel S, Graves SA, Orbay H, Ehlerding EB, Shi S, Theuer CP, Nickles RJ, Cai W. *In Vivo* tumor vasculature targeting of CuS@MSN based theranostic nanomedicine. ACS Nano. 2015; 9:3926. [PubMed: 25843647]
48. Liu Z, Rong P, Yu L, Zhang X, Yang C, Guo F, Zhao Y, Zhou K, Wang W, Zeng W. Dual-modality noninvasive mapping of sentinel lymph node by photoacoustic and near-infrared fluorescent imaging using dye-loaded mesoporous silica nanoparticles. Mol Pharmaceutics. 2015; 12:3119.
49. Walker WA, Tarannum M, Vivero-Escoto JL. Cellular endocytosis and trafficking of cholera toxin B-modified mesoporous silica nanoparticles. J Mater Chem B. 2016; 4:1254.
50. Roy LD, Sahraei M, Subramani DB, Besmer D, Nath S, Tinder TL, Bajaj E, Shanmugam K, Lee YY, Hwang SIL, Gendler SJ, Mukherjee P. MUC1 enhances invasiveness of pancreatic cancer cells by inducing epithelial to mesenchymal transition. Oncogene. 2011; 30:1449. [PubMed: 21102519]
51. Yardeni T, Eckhaus M, Morris HD, Huizing M, Hoogstraten-Miller S. Retro-orbital injections in mice. Lab Anim. 2011; 40:155.
52. Schoch A, Emrich T, Thorey IS, Engert J, Winter G. Comparison of the lateral tail vein and the retro-orbital venous sinus routes of antibody administration in pharmacokinetic studies. Lab Anim. 2014; 43:95.
53. Price JE, Barth RF, Johnson CW, Staubus AE. Injection of cells and monoclonal antibodies into mice: Comparison of tail vein and retroorbital routes. Proc Soc Exp Biol Med. 1984; 177:347. [PubMed: 6091149]
54. Steel CD, Stephens AL, Hahto SM, Singletary SJ, Ciavarra RP. Comparison of the lateral tail vein and the retro-orbital venous sinus as routes of intravenous drug delivery in a transgenic mouse model. Lab Anim. 2008; 37:26.
55. Qiao ZA, Zhang L, Guo M, Liu Y, Huo Q. Synthesis of Mesoporous Silica Nanoparticles via Controlled Hydrolysis and Condensation of Silicon Alkoxide. Chem Mater. 2009; 21:3823.
56. Beales PA, Geerts N, Inampudi KK, Shigematsu H, Wilson CJ, Vanderlick TK. Reversible assembly of stacked membrane nanodiscs with reduced dimensionality and variable periodicity. J Am Chem Soc. 2013; 135:3335. [PubMed: 23405911]
57. Nasr M, Ghorab MK, Abdelazem A. *In vitro* and *in vivo* evaluation of cubosomes containing 5-fluorouracil for liver targeting. Acta Pharmaceutica Sinica B. 2015; 5:79. [PubMed: 26579429]
58. Bertrand N, Wu J, Xu X, Kamaly N, Farokhzad OC. Cancer nanotechnology: The impact of passive and active targeting in the era of modern cancer biology. Adv Drug Delivery Rev. 2014; 66:2.
59. Stechman MJ, Ahmad BN, Loh NY, Reed AAC, Stewart M, Wells S, Hough T, Bentley L, Cox RD, Brown SDM, Thakker RV. Establishing normal plasma and 24-hour urinary biochemistry

ranges in C3H, BALB/c and C57BL/6J mice following acclimatization in metabolic cages. Lab Anim. 2010; 44:218. [PubMed: 20457824]

60. Rodriguez J, Fernandez I. Clinical biochemistry parameters in C57BL/6J mice after blood collection from the submandibular vein and retroorbital plexus. Reply. J Am Assoc Lab Anim Sci. 2010; 49:400. [PubMed: 20819382]

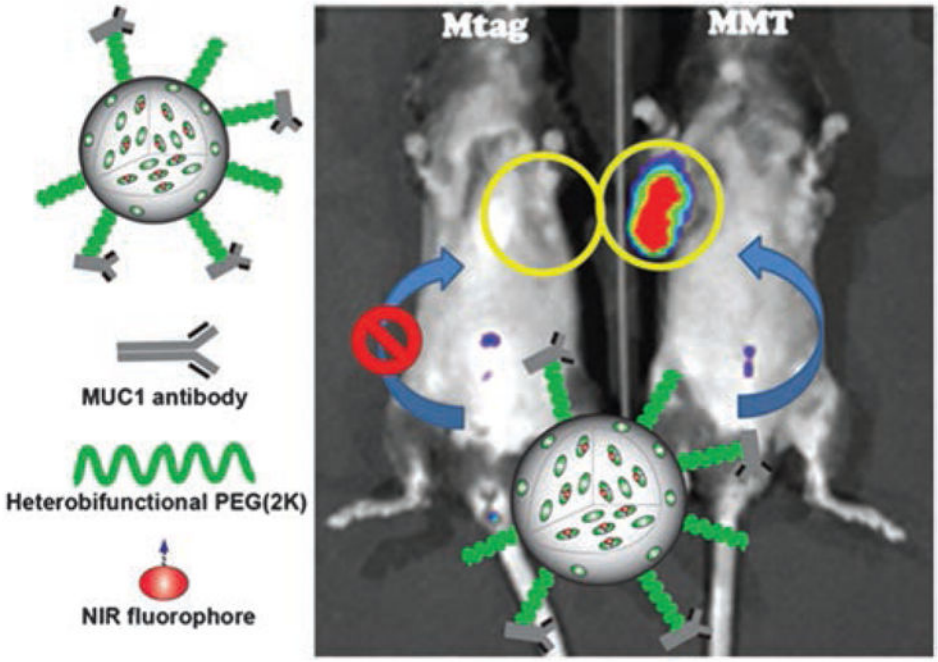

Figure 1.

Schematic representation of the tMUC1-specific dye-doped NIR fluorescent mesoporous silica nanoparticles (ab-tMUC1-NIR-MSN) optical probe developed in this work. MSNs were chemically functionalized with a NIR dye (NIR-797), heterobifunctional PEG(2K) linker and tMUC1 antibody (TAB-004™). This nanoparticulate NIR contrast imaging probe selectively accumulates in the tumor tissue of a MMT mouse that overexpress human tMUC1 antigen. On the contrary; the Mtag mouse, which also spontaneously develops breast tumor, but overexpress the mouse homolog of tMUC1 antigen, does not show significant accumulation of nanoparticles. The yellow circles indicate the localization of the largest palpable tumor mass.

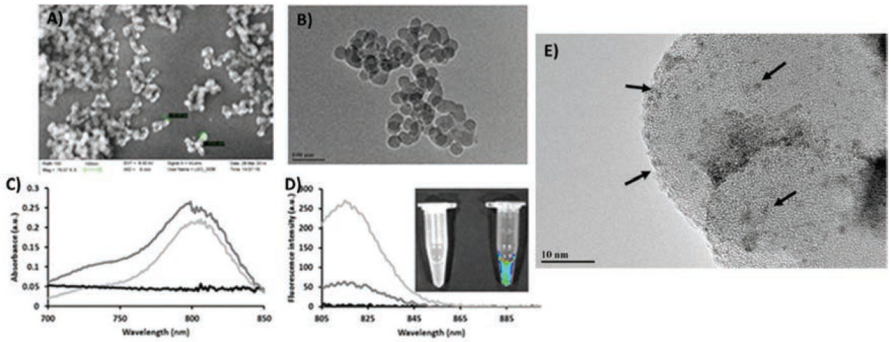

Figure 2.

Structural and photophysical characterization of MSNs and NIR MSNs. (A) Scanning and (B) transmission electron microscopy images of MSNs. (C) UV-vis-NIR spectra of MSNs (black), NIR-797 dye (light gray), and NIR-MSNs (dark gray). (D) Fluorescence emission spectra of MSNs (black), NIR-797 dye (light gray), and NIR-MSNs (dark gray). Inset: fluorescence signal from MSNs (left) and NIR-MSNs (right) taken by IVIS imaging system. (E) TEM image of negatively-stained (Nano-W) ab-tMUC1-NIR-MSNs.

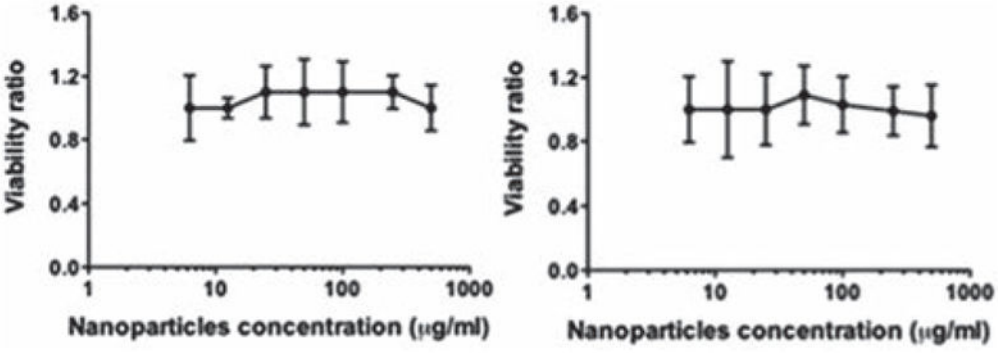

Figure 3.

Viability ratio for Mtag (left) and MMT (right) cancer cells exposed to increasing concentrations of ab-tMUC1-FITC-MSNs for 48 h. Error bars represent the standard deviation of five independent experiments.

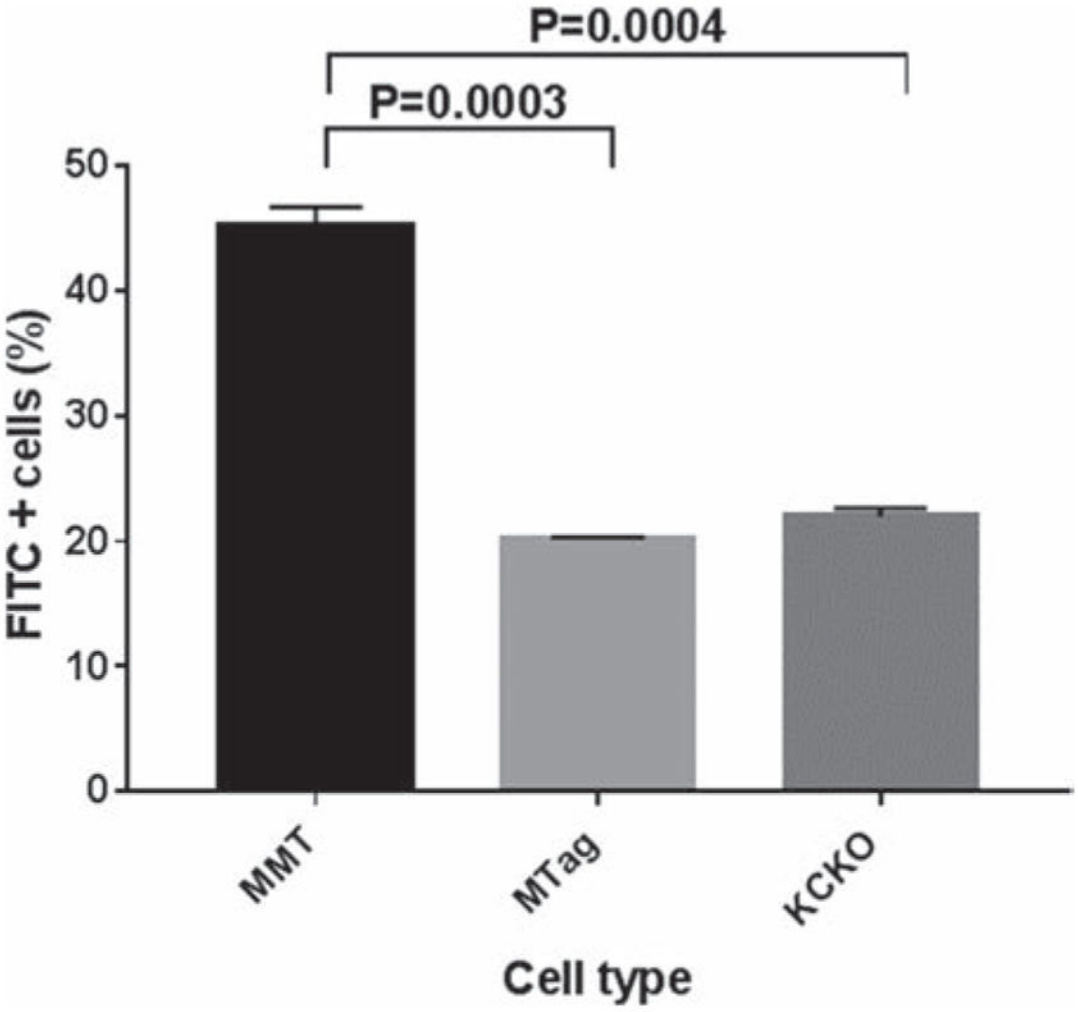

Figure 4.

Internalization of ab-tMUC1-FITC-MSNs in MMT (black), MTag (light grey) and KCKO (dark grey) cells exposed to 25 μg/mL of MSN material for 2 h. Error bars represent the SEM of three independent experiments.

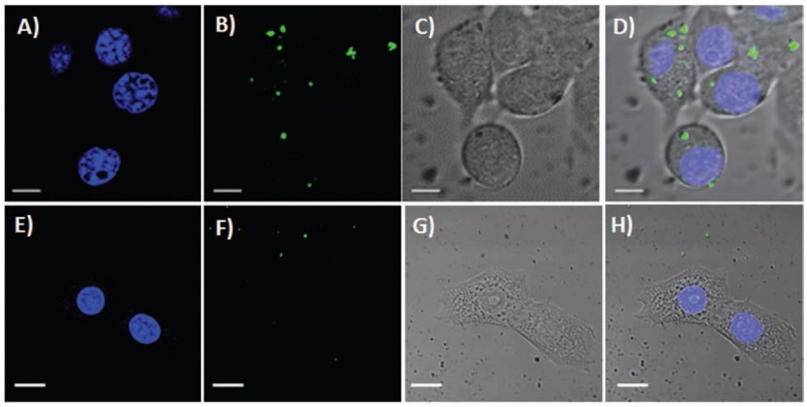

Figure 5.

Confocal microphotographs of MMT and Mtag cancer cells incubated in the presence of 100 μg/mL of ab-tMUC1-FITC-MSNs for 4 h at 37 °C. MMT (A–D) and Mtag (E–H) cells stained with the nuclear fluorophore DAPI (blue, A and E) and depicting ab-tMUC1-FITC-MSN material (green, B and F). Bright field microphotographs (C and G) are merged with DAPI stained nucleus and FITC fluorescent material (D and H). Scale bar = 5 μm.

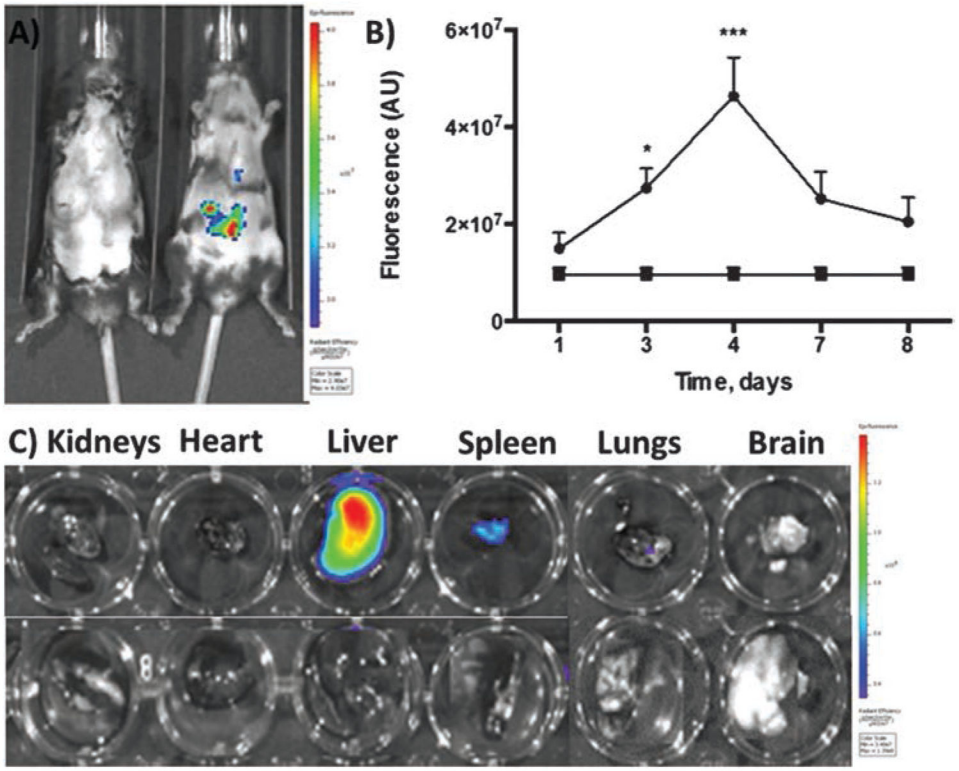

Figure 6.

Biodistribution of ab-tMUC1-NIR-MSN probe in non-tumor bearing C57BL/6 mice. (A) *In vivo* image of an injected mouse with ab-tMUC1-NIR-MSNs 3 days post-injection (right) compared with non-injected mouse (left); (B) Kinetics of fluorescence associated with ab-tMUC1-NIR-MSN material in the abdominal region of C57BL/6 mice overtime as measured by IVIS in mice injected with ab-tMUC1-NIR-MSN (filled dots) and in control mice (filled square). Repeated measured 2-way ANOVA (injection of ab-tMUC1-NIR-MSN (yes/no) and time (1 to 8 days) indicates that fluorescence on day 4-post injection was significantly higher than on day 1, 3, 7 and 8 in animals injected with ab-tMUC1-NIR-MSN. In addition, repeated measure ANOVA also confirm that at day 3 and 4 post-injection (*p<0.05 and ***p<0.001, respectively) but not at day 1, 7 or 8, fluorescence was significantly higher in the liver compared to background signal observed in non-injected animals; (C) *Ex vivo* NIR fluorescence images of isolated organs after 3 days (top) post-injection of ab-tMUC1-NIR-MSNs and control mouse (bottom).

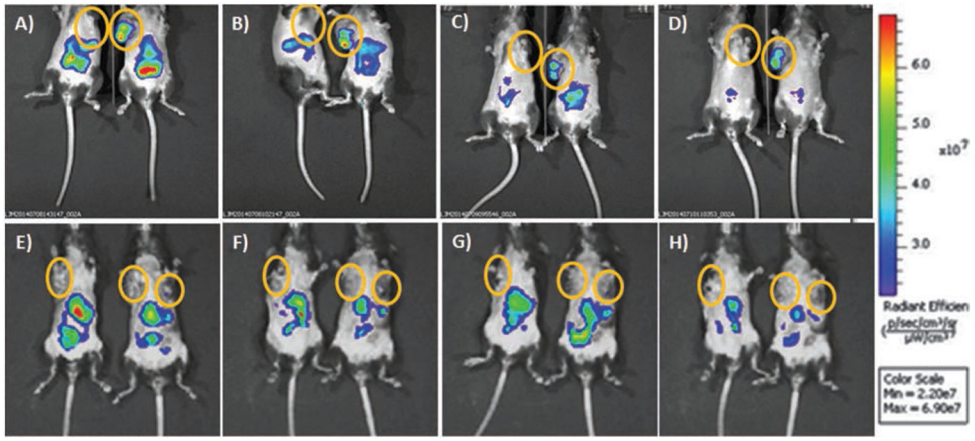

Figure 7.

Representative images of *in vivo* overtime detection of NIR fluorescence in Mtag and MMT mice. Following, RO injection of (A–D) ab-tMUC1-NIR-MSNs and (E–H) MeOPEG-NIR-MSNs. Mtag (left) and MMT (right) mice were imaged at (A/E) 5 min, (B/F) 4, (C/G) 24 and (D/H) 48 h post-injection using the IVIS system. As shown tumor masses (circles) are recognized by abtMUC1-NIR-MSNs in MMT mice only (i.e., the only one presenting the specific human tMUC-1 antigen recognized by the antibody bound to the NIR-fluorescent nanoparticle). Accumulation in the abdominal region is observed in both mouse types. The yellow circles indicate the localization of the largest palpable tumor mass.

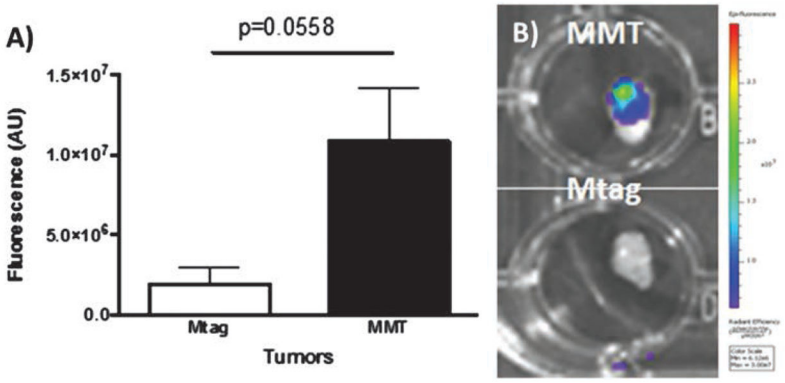

Figure 8.

(A) *Ex vivo* measurements of the fluorescence of ab-tMUC1-NIR-MSN nanoprobes in the Mtag-derived and MMT-derived tumor. Post-euthanasia, tumors were excised and the fluorescence emitted by ab-tMUC1-NIR-MSN nanoprobes (expressed as fluorescence per gram of tumor) measured using the IVIS system (A, $n = 3$ per group). (B) Representative photographs taken 48 h post ab-tMUC1-NIR-MSN injection of MMT (top) and Mtag (bottom) derived tumors are presented.

Table I

Structural characterization of the MSN-based materials.

Material	HD (nm)*	PdI	ZP (mV)	OC (%)	SA (m^2/g)
MSNs	48.7	0.14	−20.7 ± 1.3	0.5	357.6
NIR-MSNs	66.1	0.29	−11.5 ± 1.3	8.7	334.4
CPEG-NIR-MSNs	95.2	0.24	−12.5 ± 0.3	14.4	304.1
ab-tMUC1-NIR-MSNs	107.7	0.16	−2.5 ± 0.3	**	ND
MeOPEG-NIR-MSNs	93.2	0.21	−8.5 ± 0.7	15.8	285.3
FITC-MSNs	57.8	0.22	−10.3 ± 0.9	8.3	315.3
CPEG-FITC-MSNs	99.7	0.23	−13.1 ± 0.5	13.8	313.9
abMUC1-FITC-MSNs	115.2	0.29	−2.9 ± 0.4	**	ND
MeOPEG-FITC-MSNs	102.6	0.31	−6.3 ± 0.8	15.2	294.1

Notes: HD = Hydrodynamic diameter; PdI = Polydispersity index; ZP = ζ-potential; OC = Organic content; SA = Surface area;

* Data measured in phosphate buffer solution (1 mM; pH 7.4)/Concentration of MSN = 0.1 mg/mL;

* The amount of ab-tMUC1 chemically attached to NIR-MSNs was determined by the BCA assay (see text);

ND: not determined.

Table II

Liver function in control and mice injected with ab-tMUC1-NIR-MSNs.

	Control			ab-tMUC1-NIR-MSNs		
Measurement (unit)	**Sample**	**SEM**	***N***	**Sample**	**SEM**	***N***
Albumin (g/dL)	1.07	0.09	3	1.00	0.06	3
Total bilirubin (mg/dL)	0.19	0.10	3	0.23	0.14	3
Direct bilirubin (mg/dL)	0.30	0.06	3	0.27	0.12	3
Alkaline phosphatase (U/L)	83.00	21.08	3	39.00	5.51	3
AST (U/L)	131.00	31.00	2	125.00	43.92	3
ALT (U/L)	23.50	2.50	2	9.33	2.96	3
Total protein (g/dL)	2.93	0.48	3	2.73	0.09	3

Table III

Fluorescence of *ex vivo* organs as determined by IVIS imaging system and reported as arbitrary unit (AU) per gram of organ ± SEM.

	Mtag (*n* = 3) (a.u.) E-7	**MMT (*n* = 3) (a.u.) E-7**
Liver	3.40 ± 1.44	4.49 ± 2.89
Spleen	0.51 ± 0.18	0.44 ± 0.18
Kidneys	0.28 ± 0.09	0.68 ± 0.29